NLRP3 Promotes Diabetic Bladder Dysfunction and Changes in Symptom-Specific Bladder Innervation

Francis M. Hughes Jr.,[1,2] Nathan A. Hirshman,[1] Brian M. Inouye,[1] Huixia Jin,[1] Eloise W. Stanton,[1] Chloe E. Yun,[1] Leah G. Davis,[1,3] Jonathan C. Routh,[1,4] and J. Todd Purves[1,2,4]

Diabetes 2019;68:430–440 | https://doi.org/10.2337/db18-0845

The NLRP3 inflammasome senses diabetic metabolites and initiates inflammation implicated in diabetic complications and neurodegeneration. No studies have investigated NLRP3 in diabetic bladder dysfunction (DBD), despite a high clinical prevalence. In vitro, we found that numerous diabetic metabolites activate NLRP3 in primary urothelial cells. In vivo, we demonstrate NLRP3 is activated in urothelia from a genetic type 1 diabetic mouse (Akita) by week 15. We then bred an *NLRP3*$^{-/-}$ genotype into these mice and found this blocked bladder inflammation and cystometric markers of DBD. Analysis of bladder innervation established an NLRP3-dependent decrease in overall nerve density and Aδ-fibers in the bladder wall along with an increase in C-fiber populations in the urothelia, which potentially explains the decreased sense of bladder fullness reported by patients and overactivity detected early in DBD. Together, the results demonstrate the role of NLRP3 in the genesis of DBD and suggest specific NLRP3-mediated neuronal changes can produce specific DBD symptoms.

COMPLICATIONS

Diabetic bladder dysfunction (DBD) affects a large proportion of patients with diabetes, and there is currently no specific therapy to treat it (1,2). With ∼422 million people with diabetes worldwide in 2014 (3) and projections that as many as 1 in 3 people will be affected in the U.S. by 2050 (4), this represents a highly prevalent pathological condition without a targeted therapy. Patients with DBD may present with urinary frequency and urgency (i.e., overactive bladder [OAB]), detrusor underactivity and bladder decompensation (5), or some combination thereof. Although definitive longitudinal studies in humans are lacking, several experimental animal models suggest progression from OAB to decompensation (6–8). Regardless, until now, the mechanism by which the metabolic dysregulation translates into physiological dysfunction has been unclear.

It is now appreciated that diabetes is not just a disease of high blood glucose but also a disease of deranged metabolism resulting in hyperglycemia and the production of numerous metabolites such as uric acid and free fatty acids (9). These metabolites trigger inflammation that damages susceptible tissues with a resulting loss of function (10). Recent breakthroughs in other diabetic complications (nephropathy, retinopathy, and cardiomyopathy) have demonstrated this inflammation results from activation of the nucleotide-binding oligomerization domain–like receptor (NLR) NLRP3, which forms a supramolecular complex known as an inflammasome (11).

NLRP3 is the best studied of the NLR family of pattern receptors. In general, pattern receptors recognize molecules released from damaged or dying cells (or those with deranged metabolism), known as damage (or danger)–associated molecular patterns (DAMPs), or components of pathogens known as pathogen-associated molecular patterns. NLRP3 is by far the best understood NLR to recognize DAMPs and has been implicated in many diseases with a sterile inflammatory component, including diabetic complications. Upon recognition of DAMPs, via a poorly understood mechanism, NLRP3 oligomerizes and triggers enucleation of an adaptor protein known as apoptosis-associated speck-like protein C. Apoptosis-associated speck-like protein C, in turn, interacts with procaspase-1, which is cleaved and activated through an

[1]Department of Surgery, Division of Urology, Duke University Medical Center, Durham, NC
[2]Department of Bioengineering, Clemson University, Clemson, SC
[3]Duke Cancer Center Biostatistics, Duke University Medical Center, Durham, NC
[4]Department of Pediatrics, Duke University Medical Center, Durham, NC
Corresponding author: Francis M. Hughes Jr., monty.hughes@duke.edu

Received 1 August 2018 and accepted 6 November 2018

autoproteolytic process. Caspase-1, in turn, catalyzes the enzymatic maturation interleukin (IL)-1β, IL-18, and gasdermin D. Gasdermin D forms a pore in the plasma membrane, triggering a programmed necrosis called pyroptosis that releases IL-1β and IL-18 that act as proinflammatory cytokines to initiate the inflammatory response. Recently, we have shown that NLRP3 plays an important role in the urinary tract of the rodent (12,13). In the rat bladder, NLRP3 is localized to the urothelium (14,15), where it mediates sterile inflammation in several important bladder pathologies, including bladder outlet obstruction and cyclophosphamide-induced hemorrhagic cystitis (15,16). Experimental models have also implicated NLRP3 in the response to urinary tract infections (17,18). Based on the central role for NLRP3 in other diabetic complications, coupled with its importance in sterile cystitis, we hypothesized that NLRP3-mediated inflammation is a crucial element in the development of DBD.

To address this hypothesis, we bred a genetic mouse model of type 1 diabetes (the Akita mouse) (19) with a nondiabetic *NLRP3*$^{-/-}$ strain to create a novel strain of diabetic mice lacking NLRP3. These mice were then assessed for DBD. Mechanistically, DBD results, in part, from peripheral neuropathy (20,21). Therefore, we also evaluated a role for NLRP3 in the variation of nerve cell populations that could explain functional deficits in patients with diabetes, specifically diminished sensation (Aδ-fibers) and bladder overactivity (C-fibers).

RESEARCH DESIGN AND METHODS

Experimental Approach

Our approach in this study is three-pronged: *1*) in vitro analysis of the activation of the inflammasome in normal mouse urothelia by diabetic-associated DAMPs; *2*) in vivo urinary function (cystometry) in diabetic mice with a genetic deletion of NLRP3; and *3*) quantitation of nerve densities in the bladders of these mice to assess potential changes in specific nerves thought to mediate specific DBD symptoms.

Animals

All protocols adhere to the National Institutes of Health *Guide for the Care and Use of Laboratory Animals* and were approved by the Institutional Animal Care and Use Committee at Duke University Medical Center. Founder mice from The Jackson Laboratory (Bar Harbor, ME) consisted of Akita (C57BL/6J-Ins2Akita/J mice; stock number 003548) (22) and *NLRP3*$^{-/-}$ (B6.129S6-Nlrp3^{tm1Bhk}/J (stock number 021302) mice (23). Although the strain of origin for the *NLRP3*$^{-/-}$ mice (129S6/SvEvTac) is different from the Akita background (C57BL/6J), these mice have been backcrossed to C57BL/6J for >11 generations (https://www.jax.org/). Mice were bred by the Breeding Core Facility at Duke University through an independently approved protocol, and only female mice were used. All animals were genotyped by Transnetyx, Inc. (Cordova, TN) and provided to the laboratory at ~4 weeks of age.

The results of genotyping were used to assign them to one of the four experimental groups. Nondiabetics are "nondiab," and diabetics are "diab." The groups are

1. *NLRP3*$^{+/+}$, nondiab: homozygote wild-type (wt) *NLRP3* genes, homozygote wt *Ins2* genes (i.e., control mice).
2. *NLRP3*$^{+/+}$, diab: homozygote wt *NLRP3* genes; heterozygote for Akita mutation at the *Ins2* gene (i.e., Akita diabetic control).
3. *NLRP3*$^{-/-}$, nondiab: both *NLRP3* genes knocked out, homozygote wt *Ins2* genes (i.e., NLRP3 knockout control).
4. *NLRP3*$^{-/-}$, diab: both *NLRP3* genes knocked out, heterozygote for Akita mutation at the *Ins2* gene. This is the experimental mouse generated for this study.

Animals were received at 5 weeks of age. Blood glucose becomes high in Akita mice (200–300 mg/dL) ~4 weeks of age and remains high thereafter (19,24). Mice were grown to 15 weeks when DBD becomes apparent (25). No changes in urinary dysfunction were found at previous time points (25).

In Vitro Experiments

NLRP3$^{+/+}$, nondiab mice (i.e., control littermates) were used at 7 to 8 weeks of age. Urothelial cells were isolated (26) and plated (black-walled 96-well plates) at 50,000 cells/well in 90 μL complete media (F-12K media, 10% low-endotoxin dialyzed FBS, 10 μmol/L nonessential amino acids [all from HyClone Laboratories, Logan, UT], 1.0 μg/mL hydrocortisone [Sigma-Aldrich, St. Louis, MO], 10 μg/mL insulin, 5 μg/mL transferrin, and 6.7 ng/mL selenium [Gibco, Gaithersburg, MD]). Following a 24-h incubation (37°C, 95% air/5% CO_2), DAMPs (10 μL) were added and incubated as indicated. One hour prior to harvest, 1.25 mmol/L ATP was added to untreated wells. In studies that examined ATP doses, cells were plated for 24 h and then treated with 1 μg/mL lipopolysaccharide (LPS) (*Escherichia coli* 055:B5; Sigma-Aldrich) in PBS or PBS alone for 24 h before treatment with the indicated doses of ATP for 1 h. Caspase-1 activity was then measured as previously described (14). Control florescence (0 mmol/L DAMP) was subtracted from all wells and results normalized to the ATP response (except for the ATP dose-response studies).

Histological Preparation

Bladders were formalin-fixed and paraffin-embedded in a transverse orientation. Sections (5 μm) from the lower third of the bladder were stained with anti-NLRP3 (1:100) (catalog number LS-C334192; LifeSpan BioSciences, Inc., Seattle, WA), anti-PGP9.5 (1:200) (catalog number 381000; Thermo Fisher Scientific, Waltham, MA),

anti-neurofilament 200 (1:200) (NF-200; Aδ-fibers; catalog number N4142; Sigma-Aldrich), or anti–calcitonin gene-related peptide (1:80) (CGRP; C-fibers; catalog number PC205L; Calbiochem, Burlington, MA) antibodies using standard methods and citrate antigen retrieval. Staining was visualized with secondary antibodies conjugated to either Alexa Fluor 488 (NLRP3, NF-200, and CGRP) or horseradish peroxidase (PGP9.5; developed with Vectastain ABC Staining Kit; Vector Laboratories, Burlingame, CA). All sections were imaged on a Zeiss Axio Imager 2 microscope (Zeiss, Oberkochen, Germany) running Zen software (Zeiss). Tiling micrographs encompassing the entire cross section were captured by the software and stitched into a continuous image. Calibration bars were inserted and images exported as TIFF files.

FAM FLICA Caspase-1 Assay

Caspase-1 activity was assessed using the FAM FLICA Caspase-1 Assay Kit (ImmunoChemistry Technologies, Bloomington, MN) and the manufacturer's recommended protocol. Cells were analyzed on an FACSCalibur flow cytometer (BD Biosciences, San Jose, CA) (excitation 488 nm and emission 533 nm), and dot plots of forward versus side scatter were used to gate on single cells. Histograms were created, and gates were drawn to allow quantitation of the mean florescence intensity. The geometric mean of the mean florescence intensity of each sample was used for comparisons.

Blood Glucose

Blood from the submandibular vein was assessed with the AimStrip Plus blood glucose testing system (Germaine Laboratories, San Antonio, TX).

Evans Blue Dye Extravasation

Extravasation of Evans blue dye is a direct measurement of vascular permeability, which is increased during inflammation. Thus, movement of this dye into a tissue is used as an indirect measurement in inflammation (15–17,25). In this study, mice were injected (i.v.) with 10 mg/kg dye in saline and 1 h later sacrificed. Bladders were weighed and incubated overnight (56°C) in 1 mL formamide and the absorbance (620 nm) of the formamide measured. Dye amounts were calculated from a standard curve and normalized to bladder weight.

Cystometry

Awake restrained cystometry was performed (15–17,25). One week prior, suprapubic tubes (PE-10 tubing with a flared end) were implanted in the bladder and secured with a purse string suture (6–0 silk). The tube was externalized at the back of the neck. One week later, animals were placed in a Ballman-type restrainer (Natsume Seisakusho Co., Tokyo, Japan) inside of a Small Animal Cystometry Lab Station (Med Associates, St. Albans, VT) and positioned above an analytical balance to measure voided volume. The catheter was connected to a syringe pump via an in-line pressure transducer and sterile saline infused at 15 μL/min for 60–120 min. Scale and pressure readings were continuously recorded with Med-CMG software (Med Associates). After voiding cycles stabilized (typically three to four cycles), an additional three to eight cycles were recorded for quantitation. Immediately after the last void, infusion was stopped, the catheter attached to a 3-mL syringe, and the plunger was withdrawn for 10–15 s to recover any postvoid residual (PVR). CMG Analysis software (version 1.06; Med Associates) was used to analyze voiding cycles, defined as the time intravesicular pressure returned to baseline after a previous void until it returned to baseline following the next void. Voiding pressure is defined as the peak intravesical pressure, void volume as the amount of change on the scale, and frequency as the number of voids per hour. Voiding efficiency was calculated as 100 × the voiding volume divided by the bladder capacity (void volume + PVR).

Analysis of Nerve Densities

Quantitation of PGP9.5 and Aδ-nerve density in the bladder wall was carried out exactly as previously described (27), whereas quantitation of C-fibers in the urothelium required only minor modifications. Briefly, TIFF files were imported into NIS-Elements software (Nikon Co., Tokyo, Japan), calibrated, the bladder wall or urothelia layer demarcated (the region of interest), and area calculated. $PGP9.5^+$ neurons were defined as black/brown spots >50 μm^2. Aδ-fibers were defined as fluorescent areas >50 μm^2 that stained positive with a nuclear costain (DAPI). C-fibers were defined as continuous fluorescent fibers >1 μm. Neuronal density in a given section was calculated by dividing the number of nerves by the micrometers squared of the region of interest.

Statistical Analysis

All parameters were assessed by either a two-tailed Student *t* test or a one-way ANOVA followed by a Tukey post hoc analysis. Both analyses used GraphPad InStat software (GraphPad Software, La Jolla, CA), and statistical significance was defined as $P < 0.05$.

RESULTS

Diabetic DAMPs Activate the Inflammasome In Vitro

To assess the ability of diabetic DAMPs to trigger inflammasome activation, urothelial cells were treated in vitro and caspase-1 activity measured (14). ATP, the quintessential NLRP3-activating DAMP, elicited a classic dose response (Fig. 1*A*) and is subsequently used to compare other DAMPs. In most cells, NLRP3 activation requires priming with an agent such as LPS (28–34), However, LPS priming had no effect on these cells (Fig. 1*B*). Streptozotocin poisoning of β-cells is a widely used to create a type 1 model of diabetes. However, we found in Fig. 1*C* that streptozotocin directly activates the inflammasome

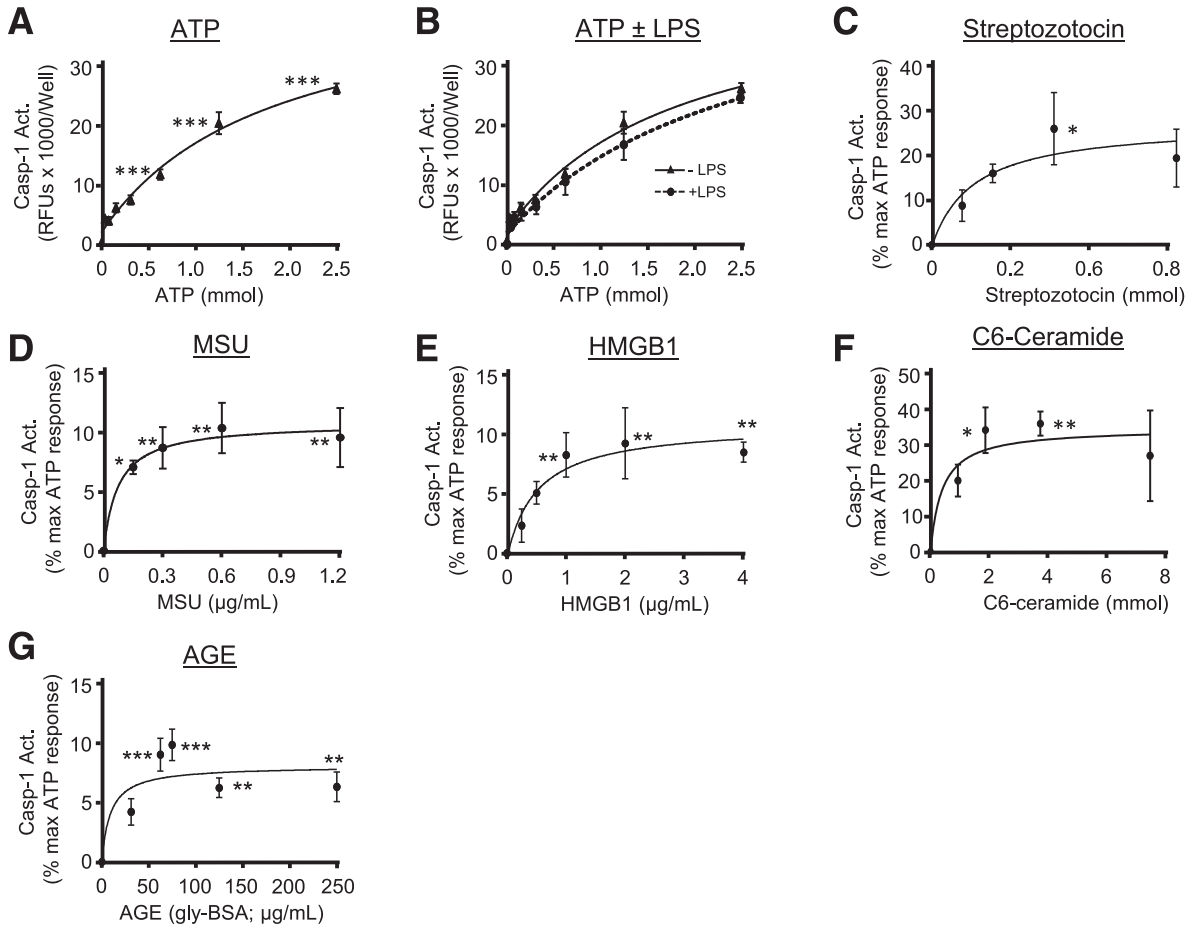

Figure 1—Analysis of various DAMPs on inflammasome activation in urothelial cells in vitro. Cells were isolated, plated, and treated with the doses of the various compounds indicated. Following incubation periods described below, caspase-1 was measured. *A*: ATP dose response. ATP was prepared as a 25 mmol/L stock in complete media (pH adjusted with 0.5 N NaOH) and dilutions made with complete media. The indicated final doses of ATP (in 10 μL) were then added to cells for 1 h prior to caspase-1 analysis. Each point represents the mean ± SEM. $n = 5$ for each dose. Asterisks indicate significant differences from 0 mmol/L control. ***$P < 0.001$ by ANOVA followed by Tukey post hoc test. *B*: Effects of LPS on the ATP dose response. Urothelial cells were plated for 24 h and then LPS (1 μg/mL) in 10 μL PBS (or PBS alone) added for an additional 24 h. Then the indicated doses of ATP were added for 1 h prior to caspase-1 analysis. It should be noted that the −LPS samples (closed triangles) are the exact same samples shown in *A*, but are included in *B* for ease of comparison. Each point represents the mean ± SEM. $n = 5$ for each dose. Student two-tailed *t* test was used to compare the −LPS and the +LPS sample at each dose of ATP. *C*: Streptozotocin dose response. Streptozotocin was prepared as a 200 mmol/L stock in 0.1 mol/L citrate buffer (pH 4.4) and dilutions made in media before being added (10 μL) to the wells at the indicated final concentrations. Cells were incubated 24 h before the addition of 1.25 mmol/L ATP for 1 h and subsequent analysis. Each point represents the mean ± SEM. $n = 5$ for each dose. *$P < 0.05$ by ANOVA followed by Tukey post hoc test. *D*: Monosodium urate (MSU) crystals (InvivoGen, San Diego, CA) were received at 5 mg/mL and dilutions prepared in complete media just prior to addition to the well (in 10 μL). Cells were incubated 24 h before the addition of 1.25 mmol/L ATP for 1 h and analysis. Each point represents the mean ± SEM. $N = 6$ for each dose. *$P < 0.05$; **$P < 0.01$ by ANOVA followed by Tukey post hoc test. *E*: High-mobility group box 1 protein (HMGB1) (ProSci, Poway, CA) was resuspended and diluted in complete media just prior to addition (10 μL) to the wells at the indicated final concentrations. Cells were incubated 24 h before the addition of 1.25 mmol/L ATP for 1 h and subsequent analysis. Each point represents the mean ± SEM. $n = 6$ for each dose. **$P < 0.01$ by ANOVA followed by Tukey post hoc test. *F*: *N*-hexanoyl-D-*erythro*-sphingosine (C6-Ceramide; Alfa Aesar, Haverhill, MA) was dissolved in DMSO and diluted in complete media prior to addition to the wells (10 μL). Cells were incubated 24 h before the addition of 1.25 mmol/L ATP for 1 h and analysis. Each point represents the mean ± SEM. $n = 6$ for each dose. *$P < 0.05$; **$P < 0.01$ by ANOVA followed by Tukey post hoc test. *G*: AGE-BSA (AGE; Calbiochem) was prepared and diluted in complete media prior to addition to the wells. Cells were incubated 24 h before the addition of 1.25 mmol/L ATP for 1 h and analysis. Each point represents the mean ± SEM. $n = 6$ for each dose. **$P < 0.01$; ***$P < 0.001$ by ANOVA followed by Tukey post hoc test. Act., activity; RFU, relative fluorescent unit.

in urothelial cells, clearly contraindicating that model for these DBD studies. Finally, Fig. 1*D–G* demonstrates activation of caspase-1 by four separate diabetic DAMPs (9): monosodium urate, high-mobility group box 1 protein, C6-ceramide, and advanced glycation end products (AGEs).

NLRP3 Is Activated During Diabetes

To explore a role for the inflammasome in DBD, it is essential to demonstrate that it is activated in the bladder by diabetes. Figure 2 demonstrates a significant increase in active caspase-1, the enzymatic readout for active inflammasomes, in urothelia from the

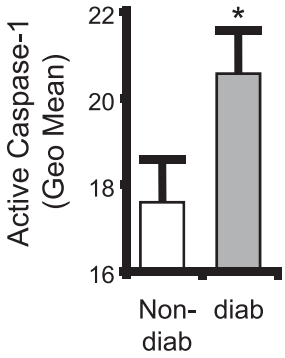

Figure 2—NLRP3 is activated in the urothelium during diabetes. Inflammasome activity (caspase-1) is increased in urothelia from diabetic mice. Urothelia were isolated and stained with a FAM FLICA Caspase-1 Assay Kit (ImmunoChemistry Technologies) as described. All mice were examined at 15 weeks of age. Bars are mean ± SEM. n = 18 (nondiabetic [non-diab]) and 17 (diabetic [diab]). *$P < 0.05$ by Student two-tailed t test. Geo Mean, geometric mean.

15-week diabetic animals compared with nondiabetic controls.

NLRP3 Is Expressed in the Mouse Urothelia, and Its Distribution Does Not Change With Diabetes

Although documented in rat (14,15), NLRP3 has never been examined in the mouse bladder. As shown in Fig. 3 (top left), expression of NLRP3 in the nondiabetic bladder was localized to the urothelial layer, identical to the rat. An indistinguishable distribution was noted in the diabetic strain (Fig. 3, top right). Isotype controls showed little background staining.

The *NLRP3*$^{-/-}$ Genotype Does Not Affect Blood Glucose in the Diabetic

To assess a role for NLRP3 in DBD, we have explored numerous end points in both nondiabetic and diabetic animals with intact *NLRP3* (*NLRP3*$^{+/+}$) and nondiabetic and diabetic mice with NLRP3 genetically deleted (*NLRP3*$^{-/-}$). Blood glucose levels in these groups are shown in Fig. 4. As expected, blood glucose levels were considerably greater in the diabetic compared with the nondiabetic mouse with NLRP3 present (*NLRP3*$^{+/+}$) (Fig. 4*A*). A similar increase with diabetes is seen with the *NLRP3*$^{-/-}$ strains (Fig. 4*B*). No significant differences were detected between the nondiabetic or diabetic based on NLRP3 expression (i.e., comparing the *NLRP3*$^{+/+}$, nondiabetic to the *NLRP3*$^{-/-}$, nondiabetic^{-}, and likewise with the diabetics). Thus, deletion of NLRP3 has no effect on blood glucose levels in either the nondiabetics or the diabetics.

Inflammation Is Present in the Diabetic Bladder and Is Mediated Through NLRP3

Although there is general evidence that inflammation is present in many tissues during diabetes, there is little or no evidence in the bladder. Therefore, we have used the Evans blue dye extravasation assay (15–17), a direct measure of vascular permeability and an indirect measure of inflammation, to gain insight into inflammation in the diabetic bladder. As shown in Fig. 5*A*, there was a significant increase of dye extravasation in the 15-week diabetic mouse compared with the nondiabetic (both *NRP3*$^{+/+}$), indicating substantial inflammation at this time point. This increase in extravasation associated with diabetes was completely blocked in the *NLRP3*$^{-/-}$ mouse (Fig. 5*B*).

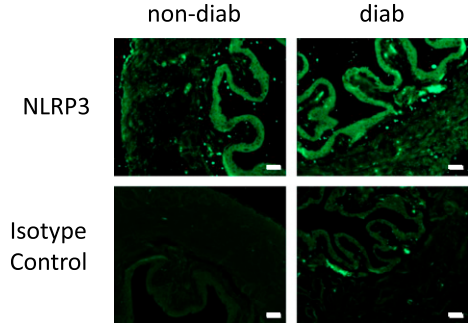

Figure 3—NLRP3 is present in mouse urothelia, and its distribution is not effected by diabetes. All mice were examined at 15 weeks of age. Sections of bladder (5 μm) from the indicated mice were stained for NLRP3 using standard immunocytochemistry and antigen retrieval protocols along with an Alexa Fluor 488–conjugated secondary antibody. Isotype controls used normal rabbit serum instead of primary antibodies. n = 3 (nondiabetic [non-diab]) and 4 (diabetic [diab]). Scale bars, 50 μm.

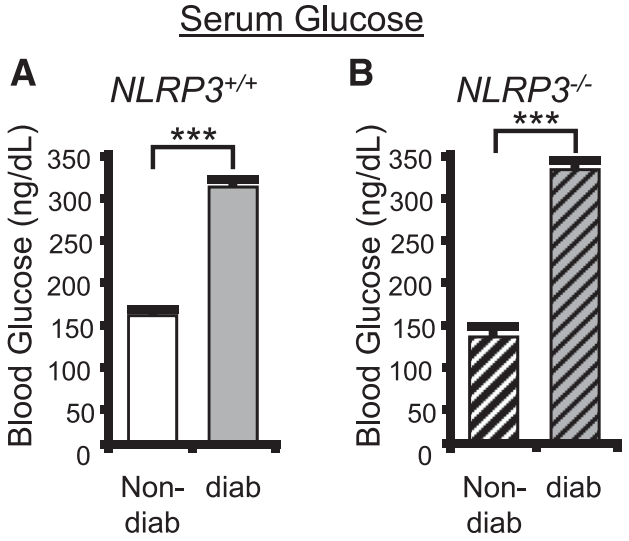

Figure 4—Blood glucose is not effected by knocking out NLRP3. Blood glucose levels were assessed at week 15 using the AimStrip Plus blood glucose testing system. *A*: Blood glucose is very significantly increased in the diabetic mouse with an *NLRP3*$^{+/+}$ genotype. n = 27 (nondiabetic [non-diab]) and 12 (diabetic [diab]). ***$P < 0.0001$ by paired Student t test. *B*: Blood glucose is significantly elevated in the diabetic mouse with an *NLRP3*$^{-/-}$ genotype. Bars are mean ± SEM. n = 18 (nondiabetic) and 21 (diabetic). ***$P < 0.0001$ by Student two-tailed t test. ANOVA followed by Tukey post hoc test was also used to compare all groups. No additional significant differences were found.

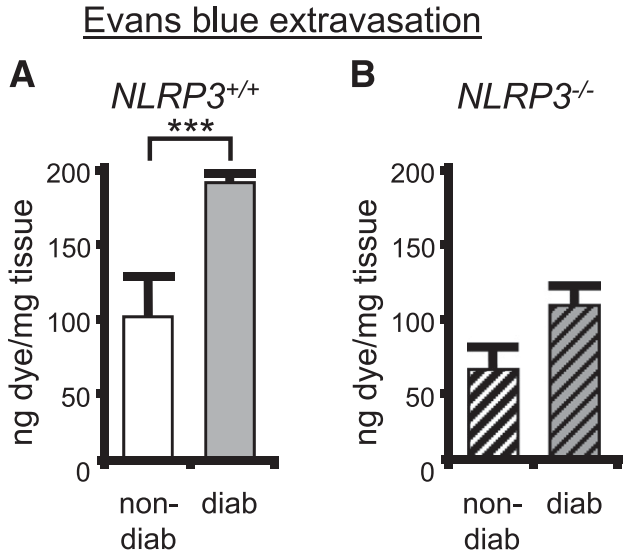

Figure 5—Inflammation is present in the diabetic bladder and mediated through NLRP3. The effect of diabetes on the induction of inflammation in the bladder was assessed in the presence and absence of NLRP3 using the Evans blue dye extravasation assay described in the Research Design And Methods section. *A*: The amount of Evans blue dye in the bladder was increased in diabetic (diab) mice compared with nondiabetic (non-diab) (both *NLRP3*$^{+/+}$). $n = 5$ (nondiabetic) and 12 (diabetic). ***$P < 0.0001$ by Student two-tailed t test. *B*: Diabetes did not affect the movement of Evans blue into the bladder in the absence of NLRP3. Bars are mean ± SEM. $n = 6$ (nondiabetic) and 16 (diabetic). ANOVA followed by Tukey post hoc test was also used to compare all groups. No additional significant differences were found.

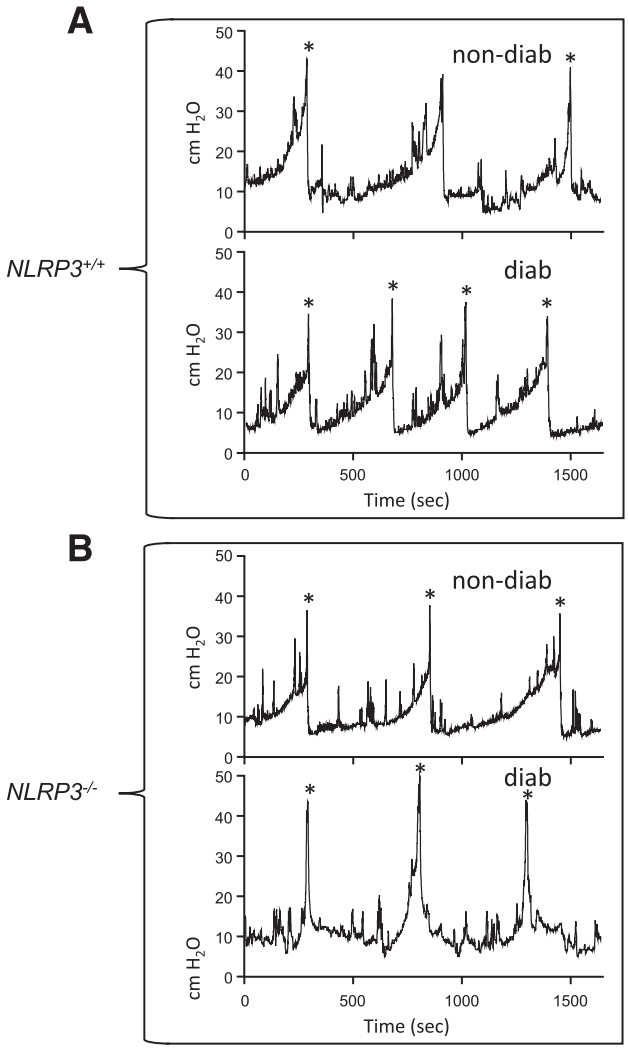

Figure 6—Representative tracings of changes in intravesicular pressures over time from the cystometry study used to demonstrate that NLRP3 is responsible for bladder dysfunction associated with DBD. Shown is a single representative tracing of the changes in luminal pressure (cm H_2O) in the bladder over several micturition cycles, obtained during cystometry, for each of the four experimental groups used in this study. These tracing were recorded using an in-line pressure transducer that made measurements every 0.25 s during the course of the experiment. The tracings were chosen to represent only several micturition cycles and do not display the entirety of the recording, which was typically much longer. Voidings correspond with the large peaks in pressure and are indicated with asterisks (*). The tracings from the four groups were arranged vertically to align the first voiding volume of each while continuing the recording for the same length of time. This was to allow easy comparison and judgement of voiding frequency (number of voids, indicated by peaks in pressure, over time). Typically, three to eight micturition cycles were quantitated per animal. *A*: Representative tracing from the NLRP3$^{+/+}$ strains. *B*: Representative tracings from the NLRP3$^{-/-}$ strains. diab, diabetic; non-diab, nondiabetic.

NLRP3 Is Responsible for Bladder Dysfunction Associated With DBD

Previously, we demonstrated that the diabetic Akita mice develop DBD by 15 weeks of age (25). To investigate the effects of NLRP3 on bladder dysfunction, we performed cystometry at this time point on the four experimental groups (35). Figure 6 shows representative tracings, for each of the four groups, of the changes in pressure (cm H_2O) in the bladder lumen during several micturition cycles. Peaks in pressure correspond with voids and are marked with an asterisk. Tracing aligns the first micturition to illustrate differences in the time between voids (the intercontraction interval), which is used to calculate voiding frequency. Not shown are tracings of the scale aligned under the rat that measure voided volume. Quantitative summaries are shown in Fig. 7. Figure 7*A* demonstrates a decrease in void volume in the diabetic mice compared with the nondiabetic when NLRP3 is present (*NLRP3*$^{+/+}$). Figure 7*B* shows an increase in voiding frequency in these same mice. In animal models, decreased void volume coupled with increased frequency are often considered synonymous with OAB, which in humans requires subjective measures (such as urgency) that cannot be measured in animals. These results are also consistent with our previous findings (25). Importantly, neither of these diabetic changes were apparent in the absence of NLRP3 (*NLRP3*$^{-/-}$) (Fig. 7*B* and *D*).

The development of DBD, although complex, is thought to progress from an early OAB phenotype to a later-stage underactive bladder (UAB) characterized by increased PVR volumes and decreased voiding efficiency (5). This UAB phenotype is indicative of a decompensated bladder. In the

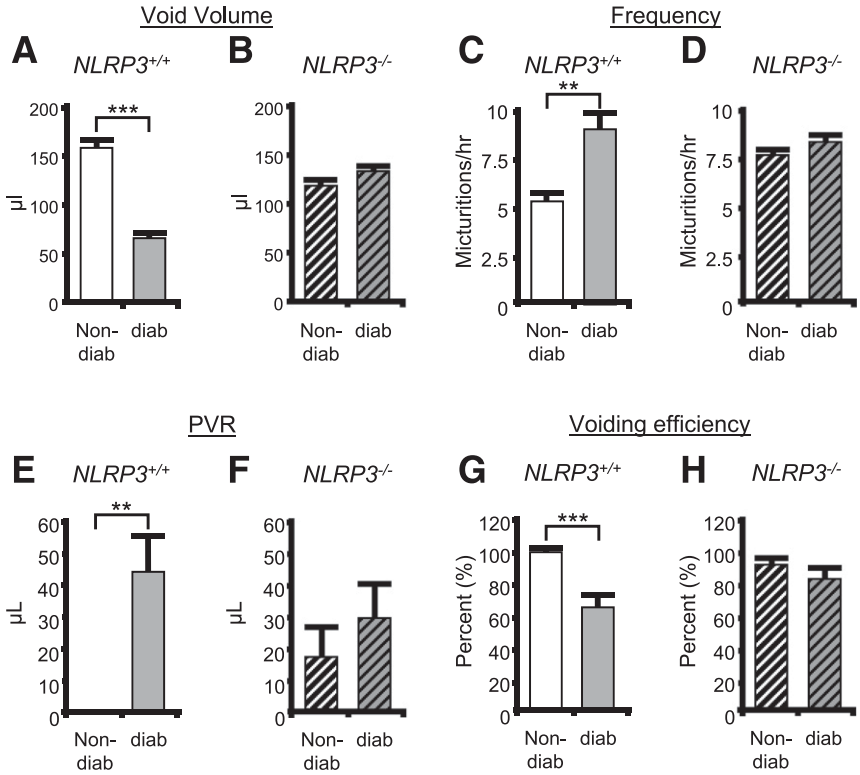

Figure 7—NLRP3 is responsible for bladder dysfunction associated with DBD. The results of various parameters measured through cystometry are shown for nondiabetic (non-diab) and diabetic (diab) mice that either express NLRP3 (*NLRP3*$^{+/+}$) or have that gene deleted (*NLRP3*$^{-/-}$). All studies were performed at 15 weeks of age, and animals were implanted with a suprapubic catheter 1 week prior to analysis. *A*: Voiding volume in nondiabetic and diabetic mice (both *NLRP3*$^{+/+}$). *B*: Voiding volume in nondiabetic and diabetic mice with NLRP3 deleted (*NLRP3*$^{-/-}$). *C* and *D*: Frequency of voiding in the indicated animals. *E* and *F*: The PVR volume, or volume of urine remaining in the bladder immediately after the last void, in the indicated animals. No PVR was ever detected in any of the nine nondiabetic/*NLRP3*$^{+/+}$ mice examined. *G* and *H*: The voiding efficiency of the indicated animals calculated as 100 (voided volume)/(voided volume + PVR). For all graphs, bars are mean ± SEM. $n = 9$ and 7 for nondiabetic and diabetic mice, respectively, that are *NLRP3*$^{+/+}$. $N = 10$ and 9 for nondiabetic and diabetic mice, respectively, that are *NLRP3*$^{-/-}$. $^{**}P < 0.01$; $^{***}P < 0.001$ by a Student two-tailed *t* test. ANOVA followed by Tukey post hoc test was also used to compare all groups for each end point. The only additional significant differences found were in void volume comparing *NLRP3*$^{+/+}$ diabetic to *NLRP3*$^{-/-}$ diabetic ($P < 0.05$) and voiding efficiency comparing *NLRP3*$^{+/+}$ diabetic to *NLRP3*$^{-/-}$ nondiabetic.

diabetic mouse at 15 weeks (Fig. 7*E* and *G*), we detected a significant increase in PVR and decrease in voiding efficiency, indicating the transition to UAB and decompensation has begun (Fig. 7*E* and *G*) (25). However, these alterations are reduced in the *NLRP3*$^{-/-}$ animals (Fig. 7*F* and *H*).

NLRP3 Controls Changes in the Densities of Nerves Related to Specific DBD Symptoms

DBD is associated with peripheral neuropathy, and one gauge of neuropathy in a tissue is the alteration in nerve number and/or density, which would be expected to decrease in diabetes and may be dependent on the NLRP3 inflammasome. To examine neuropathy in the bladder, we have quantitated total nerves using PGP9.5 as a pan neuronal marker in the bladder wall (36). Representative staining is shown in Fig. 8*A*. Arrows indicate positive staining, whereas the block arrow indicates nonspecific, or at least nonneuronal, staining of the urothelia. Although the significance of the urothelial staining is unknown, it has been previously reported (27,37). Quantitatively, the total number of nerves in the bladder wall was decreased in the diabetic mouse (Fig. 8*B*) in the presence of NLRP3, but this effect was not significant in the *NLRP3*$^{-/-}$ strain (Fig. 8*C*). There was no change of bladder wall size in any group (Fig. 8*D* and *E*), so changes in nerve density (Fig. 8*F* and *G*) directly reflect the changes in nerve number.

Next, we assessed specific nerve types thought to underlie individual bladder symptoms in patients with diabetes. First, bladder fullness is relayed to the central nervous system via Aδ-fibers, and patients often report a reduced sensation of bladder fullness. Thus, one may postulate there may be a decrease in the number and/or density of these fibers in our diabetic mice, which may be driven by the NLRP3 inflammasome. Because Aδ-fibers are predominantly in the bladder wall, we quantitated them in this compartment. Representative staining is shown in Fig. 8*H*. As shown in Fig. 8*I*, there was a significant decrease in the number of Aδ-fibers (NF-200^{+} cells) in the bladder wall of the diabetic mouse when NLRP3 was present. This decrease was not detected in the *NLRP3*$^{-/-}$ diabetics (Fig. 8*J*). Bladder wall size (Fig. 8*K* and *L*) remained

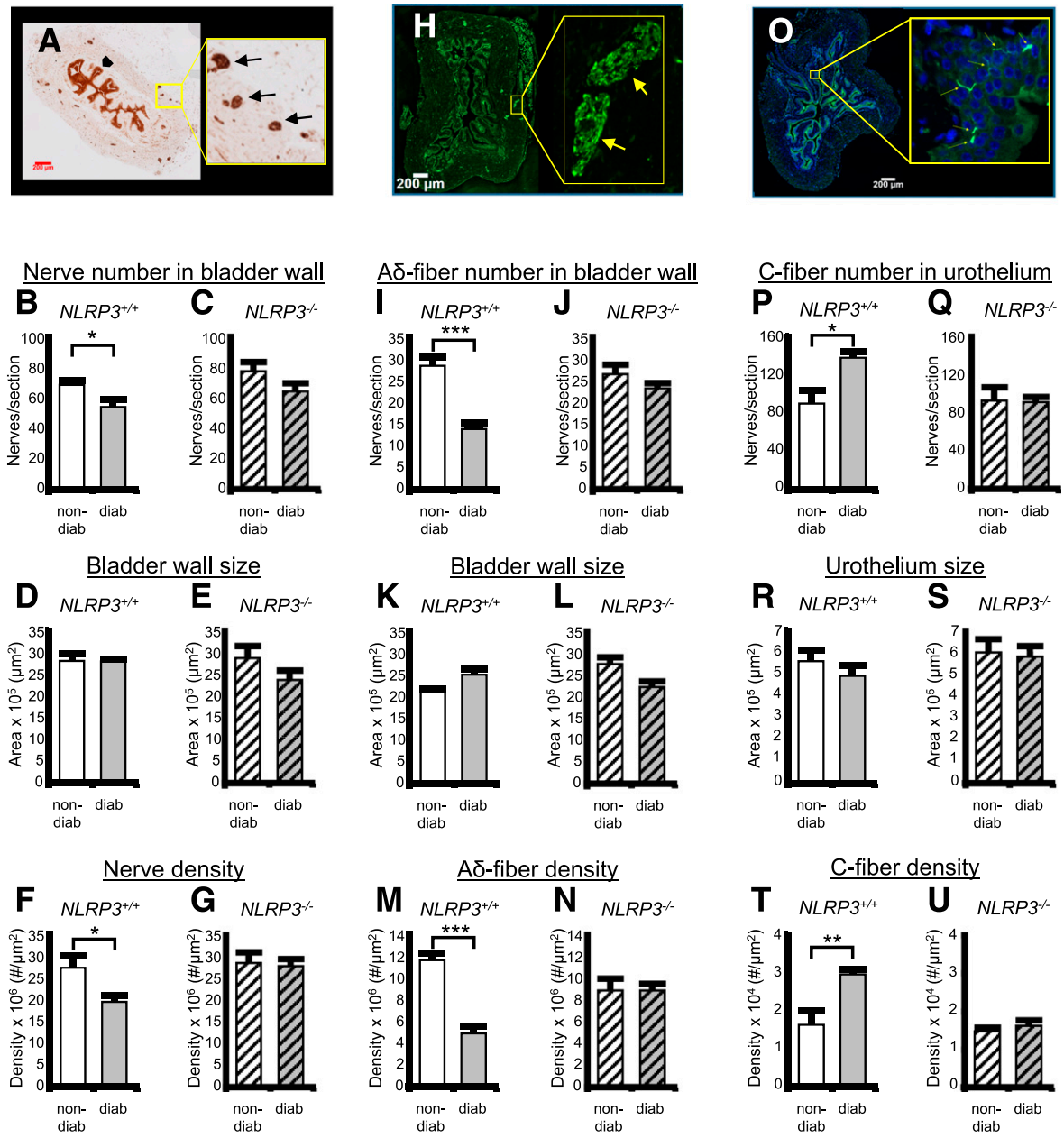

Figure 8—NLRP3 controls changes in the densities of nerves related to specific DBD symptoms. *A*: Representative micrographs of PGP9.5 staining (i.e., all neurons) in the bladder used to quantify nerves. The left micrograph depicts the entire transverse cross section stained and scanned into a TIFF file used for quantitation, as described in the RESEARCH DESIGN AND METHODS section. The yellow box indicates the area zoomed in on the right micrograph to allow better visualization. Block arrow points at urothelia that stain nonspecifically for PGP9.5, or at least are of nonneuronal origin. Arrows indicate the brown staining in the bladder wall considered to stain positive for this antigen. *B*: The number of PGP9.5$^+$ nerves in bladder wall of 15 week mice from nondiabetic (non-diab) and diabetic (diab) mice that express NLRP3 (*NLRP3*$^{+/+}$). *C*: Same analysis as *B* in mice that have the NLRP3 gene deleted (*NLRP3*$^{-/-}$). *D* and *E*: The size of the bladder wall in the same sections and groups quantitated in *B* and *C*, respectively. *F* and *G*: Density of PGP9.5$^+$ neurons in the same sections and groups quantitated in *B* and *C*, respectively. *H*: Representative micrographs of NF-200 staining (Aδ-fibers) in the bladder used to quantify nerves. The left micrograph depicts the entire transverse cross section, whereas the yellow box indicates the area zoomed in on the right, and arrows point at staining in the bladder wall considered to be positive for this antigen. *I*: The number of Aδ-fibers in bladder wall of 15 week mice from nondiabetic and diabetic mice that express NLRP3 (*NLRP3*$^{+/+}$). *J*: Same analysis as *I* in mice that have the NLRP3 gene deleted (*NLRP3*$^{-/-}$). *K* and *L*: The size of the bladder wall in the same sections and groups quantitated in *I* and *J*, respectively. *M* and *N*: Density of NF-200$^+$ neurons in the same sections and groups quantitated in *I* and *J*, respectively. *O*: Representative micrographs of CGRP staining (C-fibers) in the bladder used to quantify nerves. The left micrograph depicts the entire transverse cross section, whereas the yellow box indicates the area zoomed in on the right, and arrows point at staining in the urothelia considered to be positive for this antigen. This section is also stained with the nuclear stain DAPI in the coverslipping material to allow easier visualization. *P*: The number of C-fibers in bladder wall of 15 week mice from nondiabetic and diabetic mice that express NLRP3 (*NLRP3*$^{+/+}$). *Q*: Same analysis as *P* in mice that have the NLRP3 gene deleted (*NLRP3*$^{-/-}$). *R* and *S*: The size of the urothelia in the same sections and groups quantitated in *P* and *Q*, respectively. *T* and *U*: Density of CGRP$^+$ neurons in the same sections and groups quantitated in *P* and *Q*, respectively. For all graphs, bars represent mean ± SEM. For *B*, *D*, and *F*, $n = 11$. For *C*, *E*, and *G*, $n = 10$. For *I*, *K*, and *M*, $n = 6$. For *J*, *L*, and *N*, $n = 7$. For *P*, *R*, and *T*, $n = 4$ (non-diab) and 6 (diab). For *Q*, *S*, and *U*, $n = 3$

constant, so changes in Aδ-fiber densities (Fig. 8*M* and *N*) reflect changes in fiber number.

C-fibers are associated with an OAB phenotype (38), which is common in early stage patients with diabetes and also apparent in our mice at 15 weeks of age (Fig. 7). Thus, one may postulate there may be an increase in the number and/or density of these fibers with diabetes, and this change may be driven by NLRP3. C-fibers are predominately in the urothelia and lamina propria, and so we have focused on this tissue layer. Representative staining is shown in Fig. 8*O*. As shown in Fig. 8*P*, the number of C-fibers ($CGRP^+$) in the urothelium was significantly increased in the diabetic bladders when NLRP3 was intact. This increase did not occur in the diabetic $NLRP3^{-/-}$ mice (Fig. 8*Q*). Urothelium did not change size (Fig. 8*R* and *S*), so density results (Fig. 8*T* and *U*) again reflected changes in cell numbers.

DISCUSSION

The diabetic bladder is unique in that tissue damage can be caused by two independent mechanisms: *1*) polyuria and *2*) hyperglycemia. Previous studies (39) concluded that polyuria produced muscle hypertrophy, whereas the hyperglycemia caused tissue damage from oxidative stress. Oxidative stress often triggers inflammation, and we have recently shown diabetic bladder inflammation is due to hyperglycemia, not polyuria (25). In this study, we show that it is the NLRP3 inflammasome, located within the urothelium, that senses and responds to metabolic dysregulation by initiating an inflammatory response. Most importantly, diabetic mice lacking the NLRP3 gene do not develop DBD.

Numerous diabetic DAMPs activated the NLRP3 inflammasome in vitro, demonstrating their proinflammatory potential. Interestingly, activation of NLRP3 did not require priming as in most cell types (15). Although atypical, this has been reported (40) and suggests urothelia either do not require priming or are already primed when isolated, possibly through exposure to the commensal microbiome (40). We also found streptozotocin to be an activator of NLRP3. Streptozotocin is not a diabetic metabolite but rather a pancreatic toxin commonly used to induce diabetes in experimental models. Our results discouraged the use of that model in DBD studies.

We have recently shown that bladder inflammation and DBD develop in the Akita diabetic mouse by 15 weeks (25). In that study (and this), extravasation of Evans blue was pronounced. This study also demonstrated a concurrent activation of the inflammasome. To investigate the role of NLRP3, we crossed the Akita mouse with an $NLRP3^{-/-}$ strain to create a unique substrain of diabetic mice lacking this inflammasome. Deletion of *NLRP3* did not affect serum glucose levels, but it did abolish the inflammatory response in the diabetic. Therefore, it appears urothelial NLRP3 is indeed capable of sensing the metabolic dysregulation of diabetes and promoting an inflammatory response.

Cystometrically, our diabetic animals demonstrate clear signs of early DBD at 15 weeks with decreased voiding volume, increased frequency, and increased PVR, consistent with several prior studies (5,41). In the absence of NLRP3, diabetes did not change the frequency or void volume, unequivocally demonstrating that NLRP3 is responsible for the urinary changes of DBD. Interestingly, the diabetic bladder retained a significant PVR typically associated with later stage DBD and UAB, thus suggesting that the transition toward a decompensated state has begun. Importantly, in the absence of NLRP3, the bladder maintained normal voiding volumes and efficient emptying, showing the importance of NLRP3 in the transition to decompensation in which there is a much greater risk of complications such as infection and stone formation.

Although traditional concepts of DBD postulated that the sole pathological cause was autonomic neuropathy (42), more conventional views recognize multifactorial disturbances (43). Considering the well-known association between peripheral neuropathy and the development of DBD (44), we hypothesized that various DBD-related symptoms result from deleterious effects on the nerves within the bladder, and we found decreased nerve density in the bladder wall in the diabetic mice. Furthermore, the effects on different types of nerves vary. The Aδ-fibers, which sense fullness in the bladder, were decreased in the bladder wall, and this may explain why a diminished sense of fullness is often reported with patients with diabetes. In contrast, the C-fiber population in the urothelium increased in the diabetic bladders. C-fibers normally sense pain, but they are also associated with the emergence of an OAB phenotype (38), which is common in patients with early stage diabetes. Thus, the differential effects of inflammation on these two types of nerves provide a possible explanation for the specific symptoms associated with DBD.

The current study provides a convincing mechanism by which a plethora of diabetic insults converge on NLRP3 in the urothelia and translate into inflammation and damage to the bladder. These insults include ATP and numerous metabolites but also likely include additional insults such as reactive oxygen species, created from excessive oxidative phosphorylation, and ischemia, which is a well-known

(non-diab) and 4 (diab). $^*P < 0.05$; $^{**}P < 0.01$; $^{***}P < 0.001$ by a Student two-tailed *t* test. ANOVA followed by Tukey post hoc test was also used to compare all groups for each end point. The only additional significant differences found were in Aδ-fiber nerve number comparing $NLRP3^{+/+}$ diabetic to $NLRP3^{-/-}$ diabetic ($P < 0.05$), bladder wall size in the Aδ-fiber study comparing $NLRP3^{+/+}$ nondiabetic to $NLRP3^{-/-}$ nondiabetic ($P < 0.05$), and Aδ-fiber nerve number comparing $NLRP3^{+/+}$ diabetic to $NLRP3^{-/-}$ diabetic ($P < 0.05$). In the C-fiber studies, the $NLRP3^{+/+}$ diabetic was significantly different from both $NLRP3^{-/-}$ strains in the nerve number and density graphs ($P < 0.05$).

activator of NLRP3 that recent studies suggest plays a role in DBD (45). The signal emanating from the urothelium to trigger effects in the other bladder tissues remains unidentified but likely attributable to the major products of the inflammasome, IL-1β and IL-18, acting in a paracrine fashion. Indeed, we have shown that IL-1β is responsible for the decrease in $PGP9.5^{+}$ nerves in the bladder wall in a rat model of bladder outlet obstruction (27), whereas others have implicated it in bladder smooth muscle hypertrophy (46).

The central role of NLRP3 in development of DBD suggests a possible strategy for the prevention and management of this diabetic complication. According to the DCCT trial, only 58% of patients are able to maintain the strict glycemic control favored by the American Diabetes Association (47). Although strict regulation does prevent retinopathy, nephropathy, and other diabetic complications, bladder dysfunction still remains a problem for these patients (48–50). The current study suggests that NLRP3 inhibitors could serve as a simple means to prevent or treat DBD and possibly other diabetic complications in which this pathway plays a central role.

The results clearly show that activation of the NLRP3 inflammasome, possibly by diabetic metabolites, underlies bladder dysfunction and denervation during DBD in mice and therefore may serve as a critical pharmacological target for combating this complication in humans.

Funding. Research support was provided by the National Institute of Diabetes and Digestive and Kidney Diseases (grants K08-DK-100534 to J.C.R. and R01-DK-103534 to J.T.P.), intramural funds from Duke University, the Urology Care Foundation, and the Russell Scott, Jr., MD Urology Research Fund.

Duality of Interest. No potential conflicts of interest relevant to this article were reported.

Author Contributions. F.M.H., N.A.H., B.M.I., H.J., E.W.S., and C.E.Y. conducted experiments and acquired data. L.G.D. and J.C.R. analyzed data and performed statistical analysis. F.M.H., N.A.H., B.M.I., and J.T.P. designed the research studies and analyzed data. F.M.H. and J.T.P. wrote the manuscript. F.M.H. is the guarantor of this work and, as such, had full access to all of the data in the study and takes responsibility for the integrity of the data and the accuracy of the data analysis.

References

1. Daneshgari F, Moore C. Diabetic uropathy. Semin Nephrol 2006;26:182–185
2. Panigrahy R, Singh B, Das SK. Diabetic uropathy and bladder dysfunctions. Diabetes Metab Syndr 2017;11:81–82
3. World Health Organization. *Global Report on Diabetes*. Geneva, Switzerland, World Health Organization, 2016
4. Boyle JP, Thompson TJ, Gregg EW, Barker LE, Williamson DF. Projection of the year 2050 burden of diabetes in the US adult population: dynamic modeling of incidence, mortality, and prediabetes prevalence. Popul Health Metr 2010;8:29
5. Gomez CS, Kanagarajah P, Gousse AE. Bladder dysfunction in patients with diabetes. Curr Urol Rep 2011;12:419–426
6. Daneshgari F, Huang X, Liu G, Bena J, Saffore L, Powell CT. Temporal differences in bladder dysfunction caused by diabetes, diuresis, and treated diabetes in mice. Am J Physiol Regul Integr Comp Physiol 2006;290:R1728–R1735
7. Daneshgari F, Liu G, Birder L, Hanna-Mitchell AT, Chacko S. Diabetic bladder dysfunction: current translational knowledge. J Urol 2009;182(Suppl.): S18–S26
8. Daneshgari F, Liu G, Imrey PB. Time dependent changes in diabetic cystopathy in rats include compensated and decompensated bladder function. J Urol 2006;176:380–386
9. Shin JJ, Lee EK, Park TJ, Kim W. Damage-associated molecular patterns and their pathological relevance in diabetes mellitus. Ageing Res Rev 2015;24(Pt A): 66–76
10. Hameed I, Masoodi SR, Mir SA, Nabi M, Ghazanfar K, Ganai BA. Type 2 diabetes mellitus: from a metabolic disorder to an inflammatory condition. World J Diabetes 2015;6:598–612
11. Sepehri Z, Kiani Z, Afshari M, Kohan F, Dalvand A, Ghavami S. Inflammasomes and type 2 diabetes: an updated systematic review. Immunol Lett 2017;192:97–103
12. Inouye BM, Hughes FM Jr., Sexton SJ, Purves JT. The emerging role of inflammasomes as central mediators in inflammatory bladder pathology. Curr Urol 2018;11:57–72
13. Purves JT, Hughes FM Jr. Inflammasomes in the urinary tract: a disease-based review. Am J Physiol Renal Physiol 2016;311:F653–F662
14. Hughes FM Jr., Turner DP, Todd Purves J. The potential repertoire of the innate immune system in the bladder: expression of pattern recognition receptors in the rat bladder and a rat urothelial cell line (MYP3 cells). Int Urol Nephrol 2015; 47:1953–1964
15. Hughes FM Jr., Vivar NP, Kennis JG, et al. Inflammasomes are important mediators of cyclophosphamide-induced bladder inflammation. Am J Physiol Renal Physiol 2014;306:F299–F308
16. Hughes FM Jr., Hill HM, Wood CM, et al. The NLRP3 inflammasome mediates inflammation produced by bladder outlet obstruction. J Urol 2016; 195:1598–1605
17. Hughes FM Jr., Kennis JG, Youssef MN, Lowe DW, Shaner BE, Purves JT. The NACHT, LRR and PYD domains-containing protein 3 (NLRP3) inflammasome mediates inflammation and voiding dysfunction in a lipopolysaccharide-induced rat model of cystitis. J Clin Cell Immunol 2016;7:396
18. Hamilton C, Tan L, Miethke T, Anand PK. Immunity to uropathogens: the emerging roles of inflammasomes. Nat Rev Urol 2017;14:284–295
19. Yoshioka M, Kayo T, Ikeda T, Koizumi A. A novel locus, Mody4, distal to D7Mit189 on chromosome 7 determines early-onset NIDDM in nonobese C57BL/6 (Akita) mutant mice. Diabetes 1997;46:887–894
20. Daneshgari F, Liu G, Hanna-Mitchell AT. Path of translational discovery of urological complications of obesity and diabetes. Am J Physiol Renal Physiol 2017; 312:F887–F896
21. Deli G, Bosnyak E, Pusch G, Komoly S, Feher G. Diabetic neuropathies: diagnosis and management. Neuroendocrinology 2013;98:267–280
22. Wang J, Takeuchi T, Tanaka S, et al. A mutation in the insulin 2 gene induces diabetes with severe pancreatic beta-cell dysfunction in the Mody mouse. J Clin Invest 1999;103:27–37
23. Kovarova M, Hesker PR, Jania L, et al. NLRP1-dependent pyroptosis leads to acute lung injury and morbidity in mice. J Immunol 2012;189:2006–2016
24. Dolber PC, Jin H, Nassar R, Coffman TM, Gurley SB, Fraser MO. The effects of Ins2(Akita) diabetes and chronic angiotensin II infusion on cystometric properties in mice. Neurourol Urodyn 2015;34:72–78
25. Inouye BM, Hughes FM Jr., Jin H, et al. Diabetic bladder dysfunction is associated with bladder inflammation triggered through hyperglycemia not polyuria. Res Rep Urol 2018;10:219–225
26. Kloskowski T, Uzarska M, Gurtowska N, et al. How to isolate urothelial cells? Comparison of four different methods and literature review. Hum Cell 2014;27:85–93
27. Lütolf R, Hughes FM Jr., Inouye BM, et al. NLRP3/IL-1β mediates denervation during bladder outlet obstruction in rats. Neurourol Urodyn 2018;37:952–959
28. Bauernfeind F, Hornung V. Of inflammasomes and pathogens–sensing of microbes by the inflammasome. EMBO Mol Med 2013;5:814–826
29. Bauernfeind FG, Horvath G, Stutz A, et al. Cutting edge: NF-kappaB activating pattern recognition and cytokine receptors license NLRP3 inflammasome activation by regulating NLRP3 expression. J Immunol 2009;183:787–791

30. Franchi L, Eigenbrod T, Núñez G. Cutting edge: TNF-alpha mediates sensitization to ATP and silica via the NLRP3 inflammasome in the absence of microbial stimulation. J Immunol 2009;183:792–796
31. Gross O, Thomas CJ, Guarda G, Tschopp J. The inflammasome: an integrated view. Immunol Rev 2011;243:136–151
32. Sutterwala FS, Haasken S, Cassel SL. Mechanism of NLRP3 inflammasome activation. Ann N Y Acad Sci 2014;1319:82–95
33. Hornung V, Latz E. Critical functions of priming and lysosomal damage for NLRP3 activation. Eur J Immunol 2010;40:620–623
34. Savage CD, Lopez-Castejon G, Denes A, Brough D. NLRP3-inflammasome activating DAMPs stimulate an inflammatory response in glia in the absence of priming which contributes to brain inflammation after injury. Front Immunol 2012;3:288
35. Schneider MP, Hughes FM Jr., Engmann AK, et al. A novel urodynamic model for lower urinary tract assessment in awake rats. BJU Int 2015;115(Suppl. 6):8–15
36. Thompson RJ, Doran JF, Jackson P, Dhillon AP, Rode J. PGP 9.5–a new marker for vertebrate neurons and neuroendocrine cells. Brain Res 1983;278:224–228
37. Guan NN, Svennersten K, de Verdier PJ, Wiklund NP, Gustafsson LE. Receptors involved in the modulation of guinea pig urinary bladder motility by prostaglandin D2. Br J Pharmacol 2015;172:4024–4037
38. Fowler CJ. Bladder afferents and their role in the overactive bladder. Urology 2002;59(Suppl. 1):37–42
39. Xiao N, Wang Z, Huang Y, Daneshgari F, Liu G. Roles of polyuria and hyperglycemia in bladder dysfunction in diabetes. J Urol 2013;189:1130–1136
40. Patel MN, Carroll RG, Galván-Peña S, et al. Inflammasome priming in sterile inflammatory disease. Trends Mol Med 2017;23:165–180
41. Lee WC, Wu HP, Tai TY, Yu HJ, Chiang PH. Investigation of urodynamic characteristics and bladder sensory function in the early stages of diabetic bladder dysfunction in women with type 2 diabetes. J Urol 2009;181:198–203
42. Kaplan SA, Blaivas JG. Diabetic cystopathy. J Diabet Complications 1988;2:133–139
43. Liu G, Daneshgari F. Diabetic bladder dysfunction. Chin Med J (Engl) 2014;127:1357–1364
44. Tanik N, Tanik S, Albayrak S, et al. Association between overactive bladder and polyneuropathy in diabetic patients. Int Neurourol J 2016;20:232–239
45. Gotoh D, Torimoto K, Tatsumi Y, et al. Tadalafil, a phosphodiesterase type 5 inhibitor, improves bladder blood supply and restores the initial phase of lower urinary tract dysfunction in diabetic rats. Neurourol Urodyn 2018;37:666–672
46. Haldar S, Dru C, Choudhury D, et al. Inflammation and pyroptosis mediate muscle expansion in an interleukin-1β (IL-1β)-dependent manner. J Biol Chem 2015;290:6574–6583
47. Selvin E, Parrinello CM, Sacks DB, Coresh J. Trends in prevalence and control of diabetes in the United States, 1988-1994 and 1999-2010. Ann Intern Med 2014;160:517–525
48. Genuth S. Insights from the diabetes control and complications trial/epidemiology of diabetes interventions and complications study on the use of intensive glycemic treatment to reduce the risk of complications of type 1 diabetes. Endocr Pract 2006;12(Suppl. 1):34–41
49. Sarma AV, Kanaya A, Nyberg LM, et al.; Diabetes Control and Complications Trial/Epidemiology of Diabetes Interventions and Complications Research Group. Risk factors for urinary incontinence among women with type 1 diabetes: findings from the epidemiology of diabetes interventions and complications study. Urology 2009;73:1203–1209
50. Van Den Eeden SK, Sarma AV, Rutledge BN, et al.; Diabetes Control and Complications Trial/Epidemiology of Diabetes Research Group. Effect of intensive glycemic control and diabetes complications on lower urinary tract symptoms in men with type 1 diabetes: Diabetes Control and Complications Trial/Epidemiology of Diabetes Interventions and Complications (DCCT/EDIC) study. Diabetes Care 2009;32:664–670